Riset Geologi dan Pertambangan
Earth science journal · Open access · BRIN Earth Sciences & Maritime · BRIN Publishing
ISSN 0125-9849 e-ISSN 2354 6638

RESEARCH ARTICLE
OPEN ACCESS

Riset Geologi dan Pertambangan (2026) Vol. 36, No. 1, 99–109
DOI: 10.55981/risetgeotam.2026.1465

Keywords:
Bauxite
Geochemistry
Weathering
Gunung Kijang

Corresponding author:
Ronaldo Irzon
ronaldoirzon18@gmailcom

Article history:
Received: 06 September 2025
Revised: 23 October 2025
Accepted: 10 December 2025

Author Contributions:
Conceptualization: RI
Data curation: FD
Formal analysis: FD
Funding acquisition: FD
Investigation: FD
Methodology: FD
Supervision: RI
Visualization: RI
Writing – original draft: RI
Writing – review & editing: RI

Citation:
Irzon, R., Djabar, F., 2026. Tropical bauxitization and geochemical weathering: Evidence from stockpile and test pits of Gunung Kijang, Bintan Island. J. Ris. Geol. Pertamb., 36 (1), 99–109, doi: 10.55981/risetgeotam.2026.1465

Tropical bauxitization and geochemical weathering: evidence from stockpile and test pits of Gunung Kijang, Bintan Island

Ronaldo Irzon[1], Firdaus Djabar[2]

[1] Center for Geological Survey, Geological Agency, Jalan Diponegoro 57, Bandung, 40122, Indonesia
[2] Research Centre for Mining Technology, Nasional Research and Innovation Agency, Jalan Sangkuriang, Bandung, 40135, Indonesia

Abstract

Bauxite, the primary ore of aluminium, forms through intense weathering of alumina-rich rocks, typically in tropical climates. In Gunung Kijang, bauxite deposits were commercially mined until 2009, and remnants of these deposits are still observed in the region. This study aims to investigate the bauxitization process in the Gunung Kijang area of Bintan Island, Indonesia, with a focus on geochemical aspects. Samples from stockpile and test pits were analyzed using X-ray diffraction (XRD), X-ray fluorescence (XRF), and inductively coupled plasma mass spectrometry (ICP-MS). Geochemical results show a high concentration of gibbsite ($Al(OH)_3$). Al_2O_3 content ranged from 40.41% to 55.29%, while other oxides, such as SiO_2 and Fe_2O_3, were found in moderate concentrations. Loss on ignition (LOI) values confirmed the weathering intensity of the samples, with higher values indicating more hydroxyl-bearing minerals. Weathering indices, including the Chemical Index of Alteration (CIA) and Chemical Index of Weathering (CIW), showed that all samples experienced intense chemical weathering. Rare earth element (REE) analysis indicated Light-REE enrichment and a significant positive cerium anomaly, suggesting reductive conditions during bauxitization. The study concludes that the bauxite deposits are highly weathered and exhibit geochemical characteristics typical of tropical bauxite formation.

1. Introduction

Bauxite is a typical sedimentary rock and is economically vital as the principal ore of aluminium after separation from iron oxides, silica, and other impurities. Aluminium is one of the most applicable metals for industry on behalf of its lightweight, strength, and corrosion resistance (Ponnusamy et al., 2020; Wahid et al., 2020). Bauxite is mainly found in humid tropical to subtropical regions because it is formed after the weathering of aluminium-rich parent rocks (Heller et al., 2022; Ilijanić et al., 2023; Herawatiningsih et al., 2024). Aluminous minerals in bauxite are gibbsite (γ-$Al(OH)_3$), boehmite (γ-AlO(OH)) and diaspores (α-AlO(OH)). The type of main aluminous mineral in bauxite indicates its weathering condition, with gibbsite predominant in humid tropical regions, while boehmite is typically found in areas with tropical climates featuring extended dry seasons (Mamedov et al., 2022; Zainudeen et al., 2023; Aprillia et al., 2024). Moreover, young and porous bauxite deposits tend to be built of more gibbsite, whereas old and compacted ones contain more boehmite and diaspore (Zhang et al., 2017; Ji et al., 2022).

Indonesia has a long story of producing bauxite commodity and is ranks among the top producers globally. Indonesian bauxite mining was commercially started in the middle of

1930s (Winarno et al., 2023). Bauxite exploitation became significant for the Indonesian economy due to the newfound reserves in several other locations and the continuously increasing global demand for aluminium. The country produced 21,500,000 metric tons of bauxite in 2021, accounting for 6.28% of the world's total output (Idoine et al., *2023*). Bauxite resources are predominantly located in the western region of Indonesia (Figure 1). The most common type of bauxite in Indonesia is the lateritic bauxite which is concentrated in laterite soils. Extensive deposits of lateritic bauxite were identified in the Riau Islands, western Borneo, and central Borneo regions (Ngadenin et al., 2018; Nugraheni et al., 2023; Savko et al., 2023; Winarno et al., 2023).

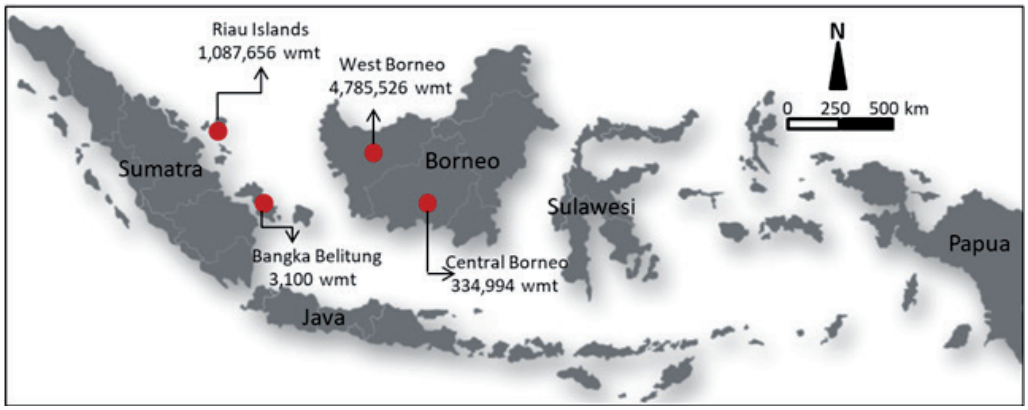

Figure 1. Reported bauxite reserves across major producing regions of western Indonesia, including the Riau Islands, Bangka Belitung, West Borneo, and Central Borneo (Direktorat Jenderal Mineral dan Batubara, 2023). Reserve tonnages shown on the map are expressed in wet metric tons (wmt).

Bauxite mining in Gunung Kijang was the first commercial mine in Indonesia and was built during the colonial period. PT Aneka Tambang, a national enterprise, took over the bauxite exploitation in 1968. The company ceased its exploitation in 2009 to focus on several post-mining operations. Environmental concerns, illegal mining by residents, and national regulation forced PT Aneka Tambang to stop the mining activities four years later (Azizah et al., 2023). However, this closure did not imply that the bauxite in Gunung Kijang was completely depleted. Abandon pits, stockpiles and bauxite-associated weathering profiles are easily found in Gunung Kijang region (Ashari et al., 2019; Azizah et al., 2023). This study aims to investigate the geochemical aspects on the bauxitization process in the Gunung Kijang area of Bintan Island.

2. Geologic setting

Bintan Island situated in the east of Sumatra near the imaginary border of Sibumasu and the East Malaya plates. The island is built of sedimentary, igneous, and metamorphic rocks (Kusnama et al., 1994). The Permo-Carboniferous Berakit Formation is oldest geological stratum and is classified as a low-grade metamorphic rock. The bedrock is found along the southwest coast of the island and is built of phyllite, slate, and schist. Granite intruded through the Berakit Formation in Triassic Age. Previous studies described that the intrusion is associated with the collision of the Sibumasu and the East Malaya plates (Irzon et al., 2020*;* Irzon et al., 2022). Granitic rock in the northern part of Bintan is pinkish and classified in the I-type based on its geochemical characteristics (Irzon et al., 2020; Irzon et al., 2021; Zulfikar et al., 2021).

Small bodies of the Miocene Andesite are identified on the central part of the island. The Guongon Formation, the island's largest rock unit, was deposited during the Plio-Pleistocene period. This 200-meter-thick sediment comprises tuffaceous sand, tuffaceous lithic, and siltstone. Holocene Alluvium is confined to a small area near Teluk Bintan. Geological features on Bintan Island include folds, joints, and faults, some of which manifest as geomorphological lineaments. Rock units of Bintan Island are drawn in Figure 2.

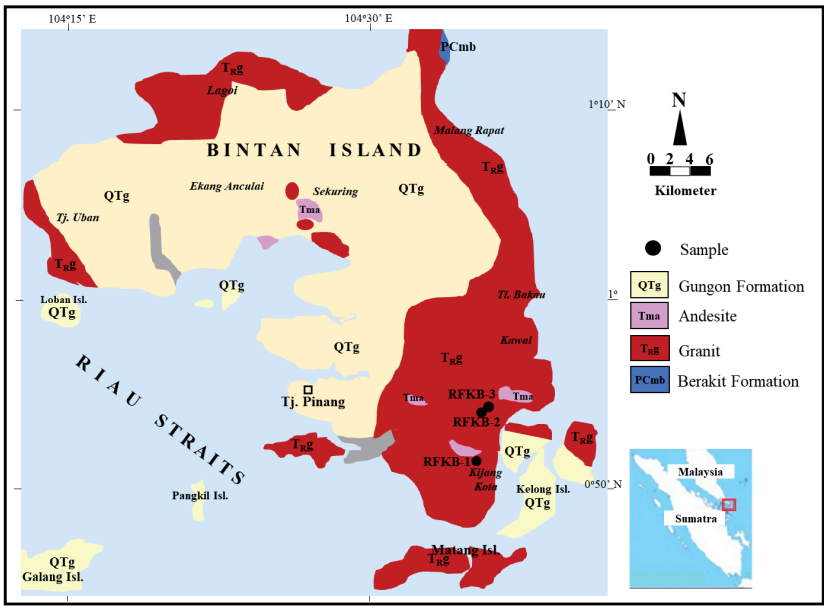

Figure 2. Geological map of the Bintan Island (based on Kusnama et al., 1994). Samples were attained in Gunung Kijang Area in the eastern region of the island.

3. Data and methods

3.1 Sample Description

All the studied samples were collected from the Gunung Kijang region, on the eastern part of Bintan Island. As a formerly PT Aneka Tambang bauxite mining area, bauxite-mining associated stockpiles and pits were easily found in Gunung Kijang (Damai et al., 2020; Melani et al., 2022). Those stockpiles may have been ignored because they did not meet the bauxite market criteria. RFKB-1 was taken from a reddish-brown stockpile located in Kijang Kota Subdistrict (Figure 3a). It was built of a combination of large, irregular chunks and finer particles of ore. Lots of spheroidal bauxite ore were identified in the sample.

RFKB-2 and RFKB-3 are laterites from two different profiles in Gunung Kijang region. The two profiles are approximately 400 m apart and excavation holes were made because they were subsurface. The test pits sampling method was adopted to recover samples and identify any changes in the horizons of the selected profile. RFKB-2 and RFKB-3 were obtained from a depth of 2 m and 1.6 m from the surface, respectively (Figure 3b & Figure 3c). A darker RFKB-2 appearance than RFKB-3 might reflect a higher mafic mineral composition. More bauxite granules were detected in RFKB-3 compared to RFKB-2.

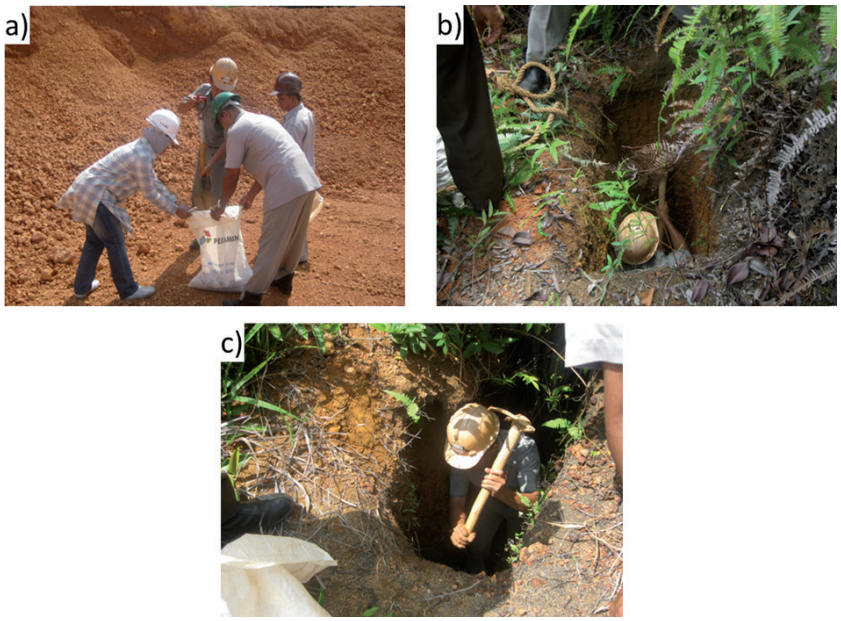

Figure 3. Field conditions of studied area: a) RFKB-1 which was taken from a stockpile; b) RFKB-2 was situated 2 m from the surface; and c) RFKB-3 of 1.6 below the surface.

3.2 Laboratory Analysis

Collected samples were sent to the laboratories of the Indonesian Geological Agency in Bandung for X-ray diffraction (XRD), X-Ray fluorescence (XRF), and Inductively Coupled Plasma – Mass Spectrometry (ICP-MS) analysis. Clay minerals characteristics and their semi-quantitative analysis were studied using the MAXIma-type Shimazu's XRD. Major oxides composition was measured by an Axios-PanAnalytical's XRF, which was used in previous studies (i.e. Irzon et al., 2019; Ainane et al., 2021; Irzon, 2022; Amin et al., 2023). Trace and rare earth elements content were evaluated using X-type Thermo Elemental's ICP-MS. The samples were not through sample washing to avoid the loss of some parts of weathering-associated minerals, but were directly dried in the oven at 105°C for at least two hours. They were then crushed by a jaw crusher before being ground and homogenised to a 150 mesh particle size using a pulveriser.

The voltage and the current of the MAXIma-type Shimazu's XRD were set at 40 kV and 35 mA, respectively. The divergent and scattering silts were adjusted at 1°, while the receiving silts were arranged at 0.30 mm. Clayey minerals were scanned continuously in the 2θ range of 4° to 80°, step size of 0.02° and at a speed of 2°/min. Samples were prepared using the pressed pellet method for measuring the composition of major oxides (SiO_2, TiO_2, Al_2O_3, Fe_2O_{3T}, MnO, CaO, MgO, K_2O, and Na_2O) by the XRF. Lost on ignition (LOI) was determined by comparing the weight of the sample after and before burning at 1000 °C as described in previous studies (Irzon et al., 2022; Irzon et al., 2023). Three acids dilution was adopted for sample destruction before Sc, V, Cr, Rb, Sr, Y, Zr, Nb, Ba, La, Ce, Pr, Nd, Sm, Eu, Gd, Tb, Dy, Ho, Er, Tm, Yb, Lu, Pb, Th, and U analysis using ICP-MS as described by Irzon (2022). Chemical composition of the selected samples is described in Tabel 1.

4. Results

Figure 4 shows the X-ray diffractograms of the three collected samples from Gunung Kijang. It can be noted that high intensity of gibbsite ($Al(OH)_3$) in all samples signifies a large alumina content. This mineral appearance also indicates a weathering process in tropic to subtropic climate region (Ali and Padmanabhan, 2017; Chen et al., 2018; Daya et al., 2021; Boeva et al., 2022). Dicktite $Al_2Si_2O_5(OH)_4$ which is a member of the kaolin group minerals was also detected in all samples to amplify the large alumina composition. The presence of gibbsite and dicktite in bauxite deposit was also reported from West Borneo (Putri et al., 2021; Hakim et al., 2023). Quartz was identified in much higher intensity on laterite samples in comparison to stockpile one.

The XRD patterns in Figure 4 reveal a systematic shift in mineral composition that reflects progressive variation in weathering intensity. RFKB-1 is dominated by gibbsite, indicated by the strong peaks at ~20°, while quartz and dickite appear only as minor phases. In contrast, RFKB-2 exhibits a more balanced assemblage in which gibbsite remains prominent but is accompanied by more pronounced dickite and quartz peaks, suggesting an intermediate weathering stage. RFKB-3 shows a trend in which quartz becomes more dominant and gibbsite decreases, while dickite persists as a subordinate component. Taken together, these patterns indicate a compositional gradation from an Al-rich, strongly lateritized horizon (RFKB-1) toward more silica-rich and less intensely weathered materials (RFKB-3).

Tabel 1. Major oxides, trace elements, and rare earth elements composition of the samples from Gunung Kijang region.

Sampel	RFKB-1	RFKB-2	RFKB-3		RFKB-1	RFKB-2	RFKB-3
	Major oxides (%)				**Trace and rare earth elements (ppm)**		
SiO_2	5.52	27.96	19.75	Sc	7.55	5.58	4.45
Reactive SiO_2	*4.29*	*10.79*	*8.56*	Y	16.10	6.36	5.49
Free SiO_2	*1.13*	*17.17*	*11.19*	La	24.01	3.29	5.12
TiO_2	0.04	0.04	0.03	Ce	57.15	14.83	16.41
Al_2O_3	55.29	40.41	49.45	Pr	4.92	0.15	0.25
Fe_2O_{3T}	8.13	10.4	5.35	Nd	86.35	22.60	23.42
MnO	0.94	0.3	0.31	Sm	7.32	2.12	1.94
CaO	0.05	0.01	0.01	Eu	1.58	0.73	0.87
MgO	0.01	0.02	0.01	Gd	18.18	24.26	13.12
Na_2O	0.03	0.04	0.04	Tb	2.93	3.97	2.02

Sampel	RFKB-1	RFKB-2	RFKB-3
K_2O	0.07	0.21	0.06
P_2O_5	0.19	0.07	0.02
LOI	29.24	20.17	24.55
Total	**99.57**	**99.73**	**99.68**
CIA	*99.61*	*99.23*	*99.70*
CIW	*99.75*	*99.79*	*99.83*
Ti/Al	0.00	0.00	0.00
Al/Na	1312.34	715.32	874.04
Ti/Na	1.08	0.81	0.61

	RFKB-1	RFKB-2	RFKB-3
Dy	3.35	0.92	0.87
Ho	5.04	2.79	2.59
Er	3.05	1.89	1.75
Tm	<LD	<LD	<LD
Yb	2.38	1.99	1.20
Lu	1.03	2.06	0.77
ToT REE	215.22	81.67	70.72
RE+Sc+Y	238.87	93.62	80.65
Ce/Ce*	1.26	5.08	3.48
Eu/Eu*	0.41	0.16	0.15

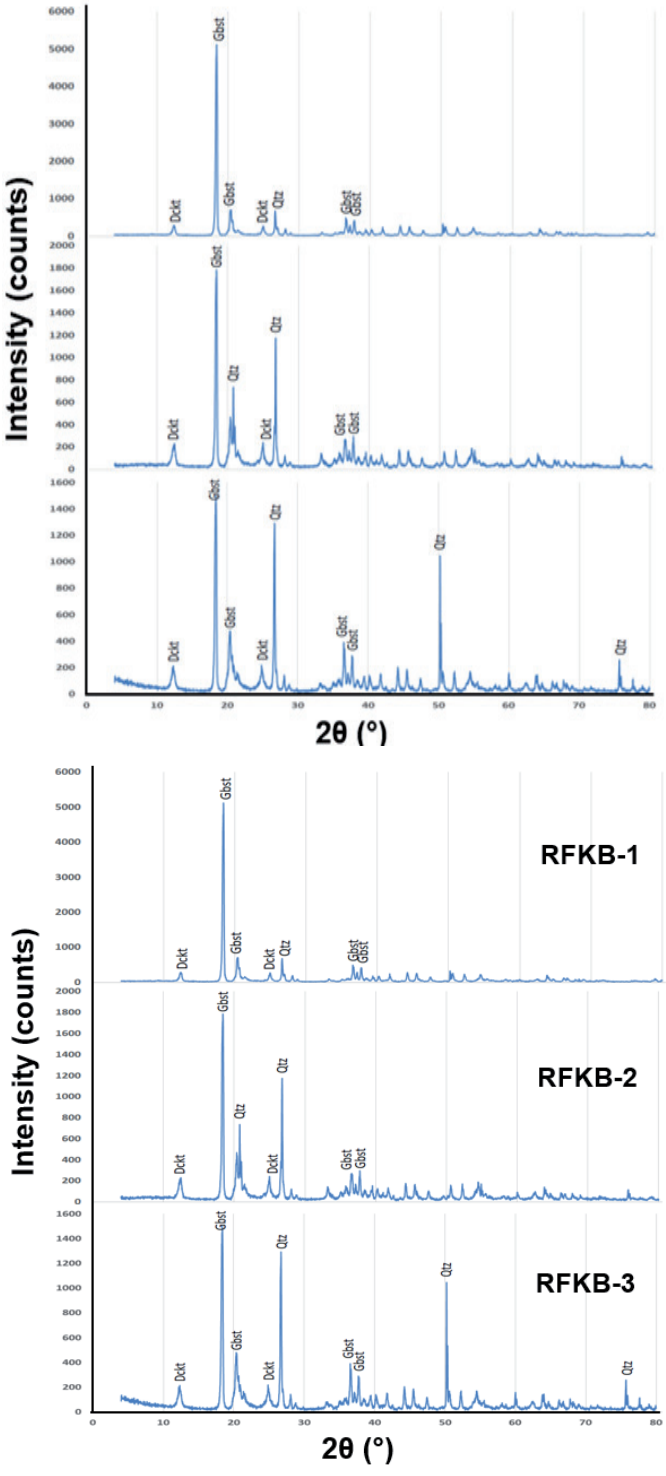

Figure 4. XRD patterns of the samples from Gunung Kijang. Gbst = gibbsite, Dckt = dicktite, and Qtz = quartz.

Al_2O_3 is the most abundant oxide of the samples ranges from 40.41% to 55.29%. Silica and Iron oxides are medium at 17.74% and 7.96% on average, respectively. Reactive silica composition in stockpile sample is much higher than the free silica with the ratio of ≈ 4:1. In contrast, both laterite samples contain more free silica than the reactive one. Other major oxides in all collected samples are relatively minor with average compositions below 1%. Stockpile sample shows the highest LOI of 29.24%, while the laterite ones of 22.52% in average. Collected samples are totally weathered due to their high LOI value of >>2%. In previous bauxite studies, LOI is linear with the amount of hydroxyl bearing minerals such as goethite, limonite, and clay (Yilmaz et al., 2018; Mucsi et al., 2021; Tchadjié et al., 2021). Higher LOI in the RFKB-01 samples express more hydroxyl-bearing minerals in the stockpile than in the laterites.

Chemical Index of Alteration (CIA) and CIW (Chemical Index of Weathering) were counted in this study on determining the extent of chemical weathering/alteration. Both proxies were adopted in previous bauxite studies (Abedini *et al.*, 2020; Nyamsari *et al.*, 2020; El Desoky *et al.*, 2022; Galmed *et al.*, 2024). CIA and CIW were calculated using Eq. 1 and Eq. 2 below:

$$CIA = \frac{Al_2O_3}{(Al_2O_3 + CaO^* + Na_2O + K_2O)} x100 \quad \text{.....(Eq. 1)}$$

$$CIW = \frac{Al_2O_3}{(Al_2O_3 + CaO^* + Na_2O)} x100 \quad \text{.....(Eq. 2)}$$

Al_2O_3, Na_2O, and K_2O in the equations above are the molecular composition of associated oxides. CaO* is the CaO abundance from the silicate fraction, whilst CaO in carbonate and phosphate minerals is excluded. The only difference between CIA and CIW is the K_2O molecular value, which is taken into account in CIA calculation but ignored for CIW. CIW is a direct index for weathering but is suitable for a process in which potassium-bearing minerals are not prevalent.

REE in this study refers to the 15 elements in the Lanthanide Series from La to Lu. The studied samples indicate medium total REE composition of 70.72 ppm to 215.22 ppm. The Light-REE (LREE; La - Eu) is averagely 91.02 ppm, while Heavy-REE (HREE, Gd-Lu) is 31.51 ppm. Nd and Ce are the three most abundant REE with average content of 44.12 ppm and 29.46 ppm, respectively. In order to eliminate the Oddo-Harkins effect, the REE abundances were normalized with the chondrite value of Boynton (1984) as shown in Figure 5. Previous studies' calculation on Ce and Eu anomalies was adopted here (Irzon and Abdullah, 2018; Mohammedyasin and Wudie, 2019; Wanas and Assal, 2021), as described in Eq. 3 and Eq. 4.

$$\frac{Ce^*}{Ce} = \frac{Ce_N}{\sqrt{(La_N \, x \, Pr_N)}} \quad \text{..... (Eq. 3)}$$

$$\frac{Eu^*}{Eu} = \frac{Eu_N}{\sqrt{(Sm_N \, x \, Gd_N)}} \quad \text{..... (Eq. 4)}$$

5. Discussion

Accumulations of Al_2O_3 and Fe_2O_{3T}, along with the depletion of SiO_2, are influenced by increased weathering intensity. This concept forms the basis of the lateritization triangular diagram (Aleva et al., 1994) on classifying kaolin, bauxite, and ferrite formation in any weathered horizons. It is shown that the sample from stockpile experienced strong lateritization, while sample from test pits underwent moderate lateritization (Figure 6a). Two samples were classified as bauxites, whilst RFKB-3 as kaolinite bauxite based on SiO_2-Fe_2O_{3T}-Al_2O_3 triangular diagram (Figure 6b). The stronger lateritization observed in the stockpile samples reflects intense and prolonged chemical weathering near the surface, where repeated leaching of SiO_2 under high rainfall and good drainage conditions promotes the residual enrichment of Al_2O_3 and Fe_2O_3. Such conditions favour the transformation of primary aluminosilicates into gibbsite and kaolinite. In contrast, the test-pit samples represent deeper horizons that have undergone less extensive leaching, resulting in only moderate lateritization. The geochemical trends—SiO_2 depletion accompanied by Al_2O_3 and Fe_2O_3 accumulation—are consistent with classic laterite profiles.

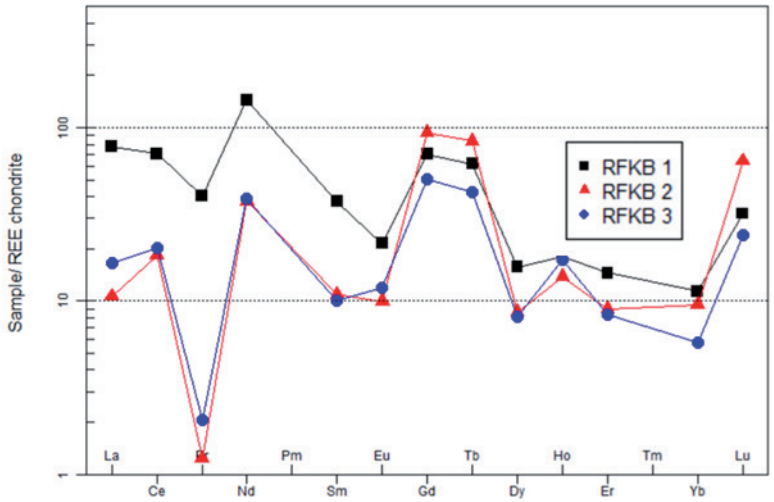

Figure 5. Spider REE diagram of the studies samples from Gunung Kijang, Bintan Island.

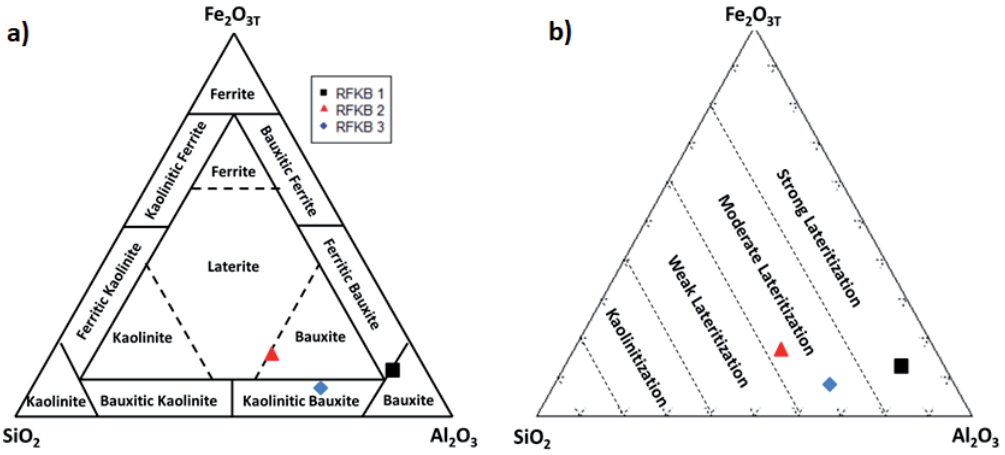

Figure 6. Plotting result of the studied samples on the triangular SiO_2-Fe_2O_{3T}-Al_2O_3 diagrams introduced by Aleva et al. (1994): a) RFKB-1 undergone strong lateritization, whilst two other samples experienced moderate lateritization; and b) RFKB-1 and RFKB-2 classified as bauxite, while the other one as kaolinitic bauxite.

Ca, Na, and K are relatively mobile elements that are resistant to leaching during weathering. On the other hand, Al and Ti are immobile and remain in the host rock. Previous elements' behaviour acts as indicators in various indices concerning the degree of alteration, such as CIA, CIW, Ti/Al, Al/Na, and Ti/Na. The CIA and CIW range for fresh rock, slightly altered, moderately altered, and highly altered rocks are <50, 50-65, 65-85, and >85, respectively (Joo et al., 2018; Tunçay et al., 2019). CIA and CIW of the samples depict close ranges of 99.23 – 99.70 (average of 99.46) and 99.78 – 99.83 (average of 99.80), respectively. Higher CIW values in comparison to CIA values are because of the absence of K_2O in the calculation. Those indexes inform that the studied samples resulted from intense chemical weathering.

An insignificant difference is observed in the Ti/Al ratio due to the samples' very low Ti but high Al compositions. Stock pile samples (RFKB-1) denote the highest Al/Na and Ti/Na ratios to define that it underwent the highest degree of weathering (Soomer et al., 2019; Zhang et al., 2023). This fact is parallel with the above SiO_2-Fe_2O_{3T}-Al_2O_3 triangular diagram (Figure 5a). As the Al/Na and Ti/Na ratios progressively increase with the degree of weathering, higher values correspond to the upper layer in a weathering profile, whilst the lower ones indicate deeper, less weathered layers (Liu et al., 2013; El Mourabet et al., 2018). Refer to those assumptions, it can be concluded that RFKB-1 is originated from uppermost strata, while RFKB-2 is the nearest to the parent rock.

REE spider diagram depicts that all three samples have a relatively similar trend. The selected samples show the LREE enrichment with decreasing composition toward the HREE. This

pattern is typical for most igneous and sedimentary rocks in which LREE concentration is higher than HREE. LREE fractionation is slight lower than the HREE fractionation refer to the main $(La/Sm)_N$ and $(Gd/Lu)_N$ of 1.57 and 1.93, respectively. The three samples show a significant positive Ce anomaly with a Ce/Ce* range of 1.26 – 5.08 (average 3.28). On the other hand, they exhibit a notable negative Eu anomaly of Eu/Eu* 0.24 on average. These facts amplify that the samples should have come from the same origin and undergone similar processes.

The rare earth elements group primarily exists in the +3 state. Certain processes and conditions including weathering, hydrothermal activity, and water circulation might induce the formation of other oxidation states, especially for Ce^{4+} and Eu^{2+}. Positive Ce anomaly in the bauxitization samples of Gunung Kijang might indicate that the cerium remained in the trivalent state (Ce^{3+}) through a reducing condition and did not precipitate out. At the same time, other REEs were moved out along with water circulation. Moreover, iron oxide minerals and aluminium hydroxides preferentially remove other REEs, including Eu, instead of Ce. This mechanism induced positive Ce anomaly but negative Eu anomaly in the studied samples.

6. Conclusions

The geochemical analysis of bauxite samples from the Gunung Kijang area, Bintan Island, reveals significant insights into the bauxitization process in this tropical region. The high concentration of gibbsite ($Al(OH)_3$) and alumina (Al_2O_3) in the samples, along with the presence of kaolin group minerals, indicates intense chemical weathering, which is characteristic of tropical climates. The high LOI values and weathering indices (CIA and CIW) confirm that the samples are highly weathered, with the stockpile sample showing the most advanced stage of weathering. The REE patterns, including the positive cerium anomaly and negative europium anomaly, suggest that the bauxitization process occurred under reducing conditions, which preserved Ce^{3+} while other REEs were leached away. The results indicate that the bauxite deposits in Gunung Kijang are not yet depleted and still contain significant alumina reserves. However, they also exhibit geochemical characteristics that suggest varied stages of weathering across different layers. This highlights the potential for further exploration and careful resource management in the region.

Acknowledgments

The writers would like to thank Mr. Edy Slameto, the head of the Center for Geological Survey of Indonesia for publication permission. Mr. Sigit Maryanto and Mr. Joko Subandrio are acknowledged for their review of the Tanggamus geology. Mrs Irfanny helped with good laboratory work.

References

Abedini, A., Mongelli, G., Khosravi, M., Sinisi, R., 2020. Geochemistry and secular trends in the middle–late Permian karst bauxite deposits, northwestern Iran. Ore Geol. Rev. 124, 103660. https://doi.org/10.1016/j.oregeorev.2020.103660

Ainane, A., Taleb, M., El-Hajjaji, F., Hammouti, B., Chetouani, A., Ainane, T., 2021. Study of dependence between two types of most abundant natural clays in Bejaad province (Central Morocco) using a statistical approach. *Mor. J. Chem.* 9, 210–220. https://doi.org/10.48317/IMIST.PRSM/morjchem-v9i2.22438

Ali, A.M., Padmanabhan, E., 2017. The impact of pH and temperature on gibbsite reactivity with quartz. *Int. J. Petrochem. Res.* 1, 40–45. https://doi.org/10.18689/ijpr-1000108

Aleva, G.J.J., 1994. Laterites: Concepts, Geology, Morphology and Chemistry. International Soil Reference and Information Centre (ISRIC), Wageningen, 169 pp

Amin, M., Sudibyo, S., Birawidha, D. C., Rinovian, A., Erlangga, B. D., Al Muttaqqi, M., Latief, A. S., Pratiwi, S., 2023. Effect of bentonite on fly ash and bottom ash based engineered geopolymer composite. *Riset Geol. Pertamb.* 33, 1225. https://doi.org/10.14203/risetgeotam2023.v33.1225

Aprillia, R., Mukhtar, W., Setiawati, S., Asbanu, G.C., Munzir, I., 2024. Genesis of Bauxite Ore in Toba Area Sanggau District, West Kalimantan Province. *J. Geocelebes* 8, 26–36. https://doi.org/10.20956/geocelebes.v8i1.30311

Ashari, I. H., Apriadi, T., Melani, W. R., 2019. Survival Rate and Growth of Economical Fishes in Tailing Ponds of Bauxite Post-mining in Senggarang, Tanjungpinang City. *Omni-Akuatika* 15, 84–91. https://doi.org/10.20884/1.oa.2019.15.2.697

Azizah, D., Hamidy, R., Mubarak, Efriyeldi, Said Raza'i, T., Muzammil, W., Pardi, H., 2023. Sustainability of mangrove forest management in the former bauxite mining area on Bintan Island. *F1000Research* 11, 179. https://doi.org/10.12688/f1000research.75932.2

Boeva, N.M., Makarova, M.A., Shipilova, E.S., Slukin, A.D., Soboleva, S.V., Zhegallo, E.A., Vishnevskaya, M.S., Bortnikov, N.S., 2022. Gibbsite and Boehmite in Weathering Crusts of Different Ages Affected by Lateritization: Location and Formation. *Dokl. Earth Sci.* 504, 353–361. https://doi.org/10.1134/S1028334X2206004X

Boynton, W.V., 1984. Cosmochemistry of the rare earth elements: meteorite studies. In: Henderson, P. (Ed.), Rare Earth Element Geochemistry. Elsevier, pp. 63–114. https://doi.org/10.1016/B978-0-444-42148-7.50008-3

Chen, J., Wang, Q., Zhang, Q., Carranza, E.J.M., Wang, J., 2018. Mineralogical and geochemical investigations on the iron-rich gibbsitic bauxite in Yongjiang basin, SW China. *J. Geochem. Explor.* 188, 413–426. https://doi.org/10.1016/j.gexplo.2018.02.010

Damai, R., Prasita, V.D., Setiawan, K.T., 2020. Monitoring changes in coral reef habitat cover on Beralas Pasir Island using Spot 4 and Spot 7 imagery from 2011 and 2018. *Int. J. Remote Sens. Earth Sci.* 17, 127–148. https://doi.org/10.30536/j.ijreses.2020.v17.a3399

Daya, A.M., Haruna, A.I., Maigari, A.S., Yahuza, I., 2021. Geology and Possible Host for Bauxite Mineralization of Mambila Plateau, NE Nigeria. *Int. J. Geoinformatics Geol. Sci.* 8, 22–28. https://doi.org/10.14445/23939206/IJGGS-V8I3P104

Direktorat Jenderal Mineral dan Batubara, 2023. Booklet promosi investasi mineral: Hilirisasi bauksit. Kementerian Energi dan Sumber Daya Mineral, Republik Indonesia, Jakarta.

El Desoky, H., Abdel Moghny, M.W., Abdel Hafez, N.A., El-Shahat, O.R., Farouk, S., Sharaka, H., 2022. Geochemical parameters for evaluating the aptian-albian kaolin deposits at abudarag region, gulf of suez: implications for the paleoclimatic conditions in the depositional environments. Iraqi Natl. J. Earth Sci. 22, 67–89. https://doi.org/10.33899/earth.2022.176211

El Mourabet, M., Barakat, A., Zaghloul, M. N., El Baghdadi, M., 2018. Geochemistry of the Miocene Zoumi flysch thrust-top basin (External Rif, Morocco): new constraints on source area weathering, recycling processes, and paleoclimate conditions. *Arab. J. Geosci.* 11, 483. https://doi.org/10.1007/s12517-018-3841-y

Galmed, M. A., Gahlan, H. A., Ghrefat, H. A., Mohamed, E. A., Al Kahtany, K. M., 2024. Petrology and geochemistry of the Az Zabirah south zone bauxite deposit at Al Ba'itha mine, north-central Saudi Arabia. *Geosci. J.* 28, 335–353. https://doi.org/10.1007/s12303-024-0004-9

Hakim, A. Y. A., Sunjaya, D., Hede, A. N. H., Indriati, T., Hidayat, T., 2023. Critical raw materials associated with the lateritic bauxite and red mud in West Kalimantan, Indonesia. *Geochem. Explor. Environ. Anal.* 23, geochem2022-064. https://doi.org/10.1144/geochem2022-064

Heller, B. M., Riffel, S. B., Allard, T., Morin, G., Roig, J. Y., Couëffé, R., Beaufort, D., Thiry, M., Selmi, S., Gautheron, C., 2022. Reading the climate signals hidden in bauxite. *Geochim. Cosmochim. Acta* 323, 40–73. https://doi.org/10.1016/j.gca.2022.01.025

Herawatiningsih, R., Krisnohadi, A., Abdillah, A. M., 2024. Impact of red mud on soil properties and revegetation species growth in bauxite mining land reclamation. *J. Degraded Min. Lands Manage.* 12, 6937–6944. https://doi.org/10.15243/jdmlm.2024.121.6937

Idoine, N.E., Raycraft, E.R., Price, F., Hobbs, S.F., Deady, E.A., Everett, P., Shaw, R.A., Evans, E.J., Mills, A.J., 2023. World Mineral Production 2017-21. British Geological Survey, Keyworth, Nottingham.

Ilijanić, N., Kovačević Galović, E., Gizdavec, N., Ivkić Filipović, I., Miko, S., Peh, Z., 2023. Geochemical records in subaerial exposure environments in Croatia using discriminant function analysis of bauxite data. *Front. Earth Sci.* 10, 1055435. https://doi.org/10.3389/feart.2022.1055435

Irzon, R., Abdullah, B., 2018. Element mobilization during weathering process of ultramafic complex in North Konawe Regency, Southeast Sulawesi based on a profile from Asera. *Indones. J. Geosci.* 5, 277–290. https://doi.org/10.17014/ijog.5.3.277-290

Irzon, R., Syafri, I., Setiawan, I., Hutabarat, J., Sendjaja, P., Haryanto, A. D., 2019. Imobilitas Unsur Tanah Jarang (UTJ) selama Mineralisasi Cu pada Granitoid Sulit Air, Provinsi Sumatra Barat. *Riset Geol. Pertamb.* 29, 185–201. https://doi.org/10.14203/risetgeotam2019.v29.1027

Irzon, R., Syafri, I., Ghani, A. A., Prabowo, A., Hutabarat, J., Sendjaja, P., 2020. Petrography and geochemistry of the Pinkish Lagoi Granite, Bintan Island: Implication to magmatic differentiation, classification, and tectonic history. *Bull. Geol. Soc. Malays.* 69, 117–129. https://doi.org/10.7186/bgsm69202010

Irzon, R., Syafri, I., Suwarna, N., Hutabarat, J., Sendjaja, P., Setiawan, V. E., 2021. Geochemistry of plutons in central Sumatra and their correlation to Southeast Asia tectonic history. *Geol. Acta* 19, 1–14. https://doi.org/10.1344/GeologicaActa2021.19.9

Irzon, R., 2022. REE-Bearing Minerals in Tin Waste Dumps of Singkep Island: Geochemical Identification and Recovery. *Indones. J. Geosci.* 9, 15–26. https://doi.org/10.17014/ijog.9.1.15-26

Irzon, R., Syaeful, H., Kusworo, A., Wahyudiono, J., Ngadenin, N., 2022. Review on Granitic Rocks in Sumatra: Intrusion Process, Classification, Mineralization, and Potential Uses. *Eksplorium* 43, 1–12. https://doi.org/10.17146/eksplorium.2022.43.1.6548

Irzon, R., Zulfikar, M., Kamiludin, U., Aryanto, N.C.D., Setiadi, D., Noviadi, Y., Hernawan, U., 2023. Geochemistry Signature and K-Ar Age of the I-type Granite at East Coast of Bangka Island. *Indones. J. Geosci.* 10, 311–326. https://doi.org/10.17014/ijog.10.3.311-326

Ji, W., Lu, Y., Zhao, C., Zhang, X., Wang, H., Hu, Z., Liu, S., Yang, Z., 2022. Mineral composition and environmental importance of Fe–Mn nodules in soils in Karst areas of Guangxi, China. *Sustainability* 14, 12457. https://doi.org/10.3390/su141912457

Joo, Y.J., Elwood Madden, M.E., Soreghan, G.S., 2018. Anomalously low chemical weathering in fluvial sediment of a tropical watershed (Puerto Rico). *Geology* 46, 691–694. https://doi.org/10.1130/G40345.1

Kusnama, Sutisna, K., Amin, T.C., Koesoemadinata, S., Sukardi& Hermanto, B., 1994. Geological Map of The Tanjungpinang Sheet, Sumatera. Scale 1:250,000. Geological Research and Development Centre - Indonesia.

Liu, B., Wang, Y., Su, X., Zheng, H., 2013. Elemental geochemistry of northern slope sediments from the South China Sea: Implications for provenance and source area weathering since Early Miocene. *Geochem.* 73, 61–74. https://doi.org/10.1016/j.chemer.2012.11.004

Mamedov, V., Boeva, N., Makarova, M., Shipilova, E., Melnikov, P., 2022. The problem of the formation of boehmite and gibbsite in bauxite-bearing lateritic profiles. *Minerals* 12, 389. https://doi.org/10.3390/min12030389

Melani, W.R., Zulfikar, A., Apriadi, T., Muzammil, W., Sabriyati, D., 2022. Characterization of hydrological aspects in Kolong Enam Retention Basin, Kijang, Bintan Island, Indonesia. *E3S Web Conf.* 339, 02010. https://doi.org/10.1051/e3sconf/202233902010

Mucsi, G., Halyag, N., Kurusta, T., Kristály, F., 2021. Control of carbon dioxide sequestration by mechanical activation of red mud. *Waste Biomass Valorization* 12, 6481–6495. https://doi.org/10.1007/s12155-021-10283-x

Mohammedyasin, M.S., Wudie, G., 2019. Provenance of the Cretaceous Debre Libanos Sandstone in the Blue Nile Basin, Ethiopia: evidence from petrography and geochemistry. *Sediment. Geol.* 379, 46–59. https://doi.org/10.1016/j.sedgeo.2018.11.003

Ngadenin, Widana, K.S., Karunianto, A.J., 2018. Study on Thorium Occurences in The Laterite Bauxite Deposits in Singkep Island in Connection With Development of Thorium Exploration in The Tin Belt Granite Area. *Eksplorium* 39, 17–26. https://doi.org/10.17146/eksplorium.2018.39.1.4204

Nugraheni, R. D., Anggraini, W., Setiawan, N. S., Riyandhani, C. P., Syavitri, D., Sunjaya, D., Hakim, A. Y. A., Sukadana, I. G., 2023. Multispectral Remote Sensing to Delineate the Distribution Area of Scandium-Bearing Minerals in Bauxite Mining Sites, West Kalimantan Province, Indonesia. *Rud.-Geol.-Naft. Zb.* 38, 13–29. https://doi.org/10.17794/rgn.2023.1.2

Nyamsari, D. G., Yalcin, M. G., Wolfson, I., 2020. Alteration, chemical processes, and parent rocks of Haléo-Danielle Plateau bauxite, Adamawa–Cameroon. *Lithol. Miner. Resour.* 55, 231–243. https://doi.org/10.1134/S002449022003004X

Putri, A. R. H., Setijadji, L. D., Sunjaya, D., 2021. Potential Enrichment of Scandium in Bauxite Deposit for the Emerging Green Technology Needs. *Indones. J. Econ. Geol.* 1, 1–12. https://doi.org/10.51835/ijeg.2021.1.1.339

Ponnusamy, P., Rahman Rashid, R. A., Masood, S. H., Ruan, D., Palanisamy, S., 2020. Mechanical properties of SLM-printed aluminium alloys: a review. *Materials* 13, 4301. https://doi.org/10.3390/ma13194301

Savko, A. D., Ovchinnikova, M. Y., 2023. Evolution of Bauxite Accumulation in the Phanerozoic. *Dokl. Earth Sci.* 513, S155–S174. https://doi.org/10.1134/S1028334X23602165

Soomer, S., Somelar, P., Mänd, K., Driese, S. G., Lepland, A., Kirsimäe, K., 2019. High-CO2, acidic and oxygen-starved weathering at the Fennoscandian Shield at the Archean-Proterozoic transition. *Precambrian Res.* 327, 68–80. https://doi.org/10.1016/j.precamres.2019.02.023

Tchadjié, L. N., Ekolu, S. O., Quainoo, H., Tematio, P., 2021. Incorporation of activated bauxite to enhance engineering properties and microstructure of volcanic ash geopolymer mortar composites. *J. Build. Eng.* 41, 102384. https://doi.org/10.1016/j.jobe.2021.102384

Tunçay, T., Dengiz, O., Bayramin, I., Kilic, S., Baskan, O., 2019. Chemical weathering indices applied to soils developed on old lake sediments in a semi-arid region of Turkey. *Eurasian J. Soil Sci.* 8, 60–72. https://doi.org/10.18393/ejss.504933

Wahid, M. A., Siddiquee, A. N., Khan, Z. A., 2020. Aluminum alloys in marine construction: characteristics, application, and problems from a fabrication viewpoint. Mar. Syst. Ocean Technol. 15, 70–80. https://doi.org/10.1007/s40868-020-00074-w

Winarno, T., Ali, R. K., Simangunsong, H., 2023. Characteristics and Genesis of Laterite Bauxite in Sompak District and Surrounding Areas, Landak Regency, West Kalimantan. *Indones. J. Geosci.* 10, 87–100. https://doi.org/10.17014/ijog.10.1.87-100

Wanas, H. A., Assal, E. M., 2021. Provenance, tectonic setting and source area-paleoweathering of sandstones of the Bahariya Formation in the Bahariya Oasis, Egypt: An implication to paleoclimate and paleogeography of the southern Neo-Tethys region during Early Cenomanian. *Sediment. Geol.* 413, 105822. https://doi.org/10.1016/j.sedgeo.2020.105822

Yılmaz, V. M., Tunç Parlak, T., Yıldız, K., 2018. Dehydroxylation of high-energy ball-milled diasporic bauxite. *J. Therm. Anal. Calorim.* 134, 135–141. https://doi.org/10.1007/s10973-018-7243-y

Zainudeen, N. M., Mohammed, L., Nyamful, A., Adotey, D., Osae, S. K., 2023. A comparative review of the mineralogical and chemical composition of African major bauxite deposits. *Heliyon* 9, e18501. https://doi.org/10.1016/j.heliyon.2023.e18501

Zulfikar, M., Nurdin, N., Aryanto, N. C. D., Syafri, I., Muljana, B., Nur, A. A., 2021. Distribution of Subsurface Quaternary Sediment in South Bintan Island Waters as A Potential Heavy Mineral Placer or Rare Earth Element Deposit Based on Seismic Interpretation. Bull. Mar. Geol. 36, 1–13. https://doi.org/10.32693/bomg.36.1.2021.698

Zhang, L., Park, C., Wang, G., Wu, C., Santosh, M., Chung, D., Song, Y., 2017. Phase transformation processes in karst-type bauxite deposit from Yunnan area, China. *Ore Geol. Rev.* 89, 407–420. https://doi.org/10.1016/j.oregeorev.2017.06.012

Zhang, M., Gong, Z., Li, J., Pan, Y., Jin, Q., Huang, C., 2023. REE mineralization related to weathering of the late Permian Emeishan basalts. *J. Geochem. Explor.* 245, 107146. https://doi.org/10.1016/j.gexplo.2022.107146